

Diffuse-interface description of strain-dominated morphology of critical nuclei in phase transformations

Lei Zhang^a, Long-Qing Chen^b, Qiang Du^{a,b,*}

^a Department of Mathematics, Pennsylvania State University, PA 16802, USA

^b Department of Materials Science and Engineering, Pennsylvania State University, PA 16802, USA

Received 3 January 2008; received in revised form 26 March 2008; accepted 26 March 2008

Available online 27 April 2008

Abstract

A diffuse interface model combined with the minimax technique is implemented to predict the morphology of critical nuclei during solid to solid phase transformations in both two and three dimensions. It takes into account the anisotropic interfacial energy as well as the anisotropic long-range elastic interactions. It is demonstrated that the morphology of critical nuclei in cubically anisotropic solids can be efficiently predicted by the computational model without a priori assumptions. A particular example of cubic to cubic transformation within the homogeneous modulus approximation is considered. The effect of elastic energy contribution on the size and shape of a critical nucleus is studied. It is shown that strong elastic energy interactions may lead to critical nuclei with a wide variety of shapes, including plates, needles and cuboids with non-convex interfaces.

© 2008 Acta Materialia Inc. Published by Elsevier Ltd. All rights reserved.

Keywords: Nucleation; Critical nuclei; Phase field modeling; Anisotropic elasticity; Solid state phase transformation

1. Introduction

Nucleation takes place when a material becomes thermodynamically metastable with respect to its transformation to a new state (solid, liquid and gas) or new crystal structure. Some common nucleation phenomena include formation of liquid droplets in a saturated vapor, appearance of ordered domains in a disordered solid and nucleation of tetragonal variants in a cubic matrix. Very often, it is the nucleation process that dictates the microstructure of a material.

In the classical theory of nucleation, the thermodynamic properties of a nucleus are assumed to be uniform and the same as in the corresponding bulk phase at equilibrium. The interface between a nucleus and the parent phase is considered to be sharp. The calculation of a critical nucleus

size is then determined by the competition between the bulk free energy reduction and the interfacial energy increase. For instance, the total free energy change accompanying the formation of a new particle is given by

$$\Delta E_{\text{total}} = \text{Volume} \cdot \Delta f_v + \text{Area} \cdot \gamma$$

where Δf_v is the bulk free energy driving force per unit volume and γ is the interfacial energy per unit area between a nucleus and the parent matrix. For a spherical particle of radius r ,

$$\Delta E_{\text{total}} = \frac{4}{3}\pi r^3 \Delta f_v + 4\pi r^2 \gamma$$

with $\Delta f_v < 0$ and $\gamma > 0$ for a given phase transformation. A nucleation event takes place by overcoming the minimum energy barrier which leads to the critical size $r^* = -2\gamma/\Delta f_v$ of the nucleus obtained as a stationary point of ΔE_{total} . The associated critical free energy of the formation of a critical nucleus, $\Delta E_{\text{total}}^*$, is then given by $\Delta E_{\text{total}}^* = 16\pi\gamma^3/3(\Delta f_v)^2$. Hence, the nucleation rate of the critical nucleus per unit volume and unit time has the form

* Corresponding author. Address: Department of Mathematics, Pennsylvania State University, University Park, PA 16802, USA.

E-mail addresses: zhang_l@math.psu.edu (L. Zhang), lqc3@psu.edu (L.-Q. Chen), qdu@math.psu.edu (Q. Du).

$I = I_0 \exp[-\Delta E_{\text{total}}^*/k_{\text{BT}}]$ with the pre-exponential factor I_0 calculated from the fundamental statistical approaches, k_{B} the Boltzmann's constant and T the absolute temperature.

While it is reasonable to assume spherical shapes for nuclei during fluid to fluid phase transitions, the morphology of critical nuclei in solids is expected to be strongly influenced by anisotropic interfacial energy and anisotropic elastic interactions. For example, nuclei for γ' precipitates in Ni-alloys can be cuboidal or spherical depending the lattice mismatch between the precipitate and matrix, θ' precipitates in Al–Cu are plates and the β' precipitates in Al–Mg–Si alloys are needle-shaped. The morphology of a critical nucleus in the presence of interfacial energy anisotropy alone can be deduced from the well-known Wulff construction. However, predicting the shape of a critical nucleus in the presence of both elastic energy and surface energy anisotropy is particularly challenging since elastic energy contribution depends on the morphology of a nucleus and lattice mismatch between the nucleus and the matrix. As a result, prior applications of the classical nucleation theory to solid state transformations typically make assumptions on the shape of a nucleus as an a priori, and the elastic energy contribution to nucleation is included as an extra barrier for nucleation, which is proportional to volume, i.e. $a^* \sim -\beta^* \gamma / (\Delta f_v + E_{\text{el}})$ where a^* represents the critical size of a nucleus, Δf_v is the bulk driving force for nucleation, β^* is a numerical factor depending on the shape of the nucleus and E_{el} is the elastic strain energy contribution to nucleation on the order of $C\epsilon_0^2$ where C is the elastic modulus and ϵ_0 is the lattice mismatch strain (transformation strain, eigenstrain, stress-free strain) between the nucleus and the matrix.

Another theoretical approach to nucleation is based on the diffuse-interface description, also called the non-classical nucleation theory. In this approach, the properties within a nucleus are inhomogeneous and the interface between the nucleus and parent matrix is diffuse. Following the seminal work of Cahn and Hilliard [1], the diffuse-interface approach has been previously applied to nucleation in solids. For example, Roitburd et al. [32] and Khachaturyan et al. [20,22] described the nucleation of a new phase in solid solutions and the general problem of extreme states of solid solutions using the diffuse interface model. More recently, Roy et al. [33] discussed the nucleation in the presence of a general long-range interaction. The focus is on the critical order parameter profiles rather than predicting the morphology of a nucleus. Wang and Khachaturyan [38] examined the morphology of nuclei during a martensitic transformation by switching on and off Langevin noise. The particles obtained using this approach do not necessarily correspond to saddle point configurations associated with a critical nucleus. Poduri and Chen [29] studied the nucleation of an ordered precipitate from a disordered matrix by extending the diffuse-interface theory of Cahn and Hilliard. Roitburd [31] and Chu et al. [5] were the first to explore the nucleation of martensites using the non-clas-

sical approach. More recently, Gagne et al. [12] studied the morphological evolution using Langevin simulations of martensitic transformations in two dimensions. They concluded that systems with long-range interactions quenched into a metastable state near the pseudo-spinodal exhibit nucleation that is qualitatively different from classical nucleation near the coexistence curve. It is noted that all existing diffuse interface theories for nucleation in solids ignore the anisotropic interfacial energy and anisotropic long-range elastic interactions. Within the phase-field approach, nucleation during solidification has been studied by Granasy et al. [14,15], and nucleation in solids in the presence of elastic interactions by Hu and Chen [18], Zhang et al. [41], Shen et al. [35] and Luo et al. [27]. Using a microscopic model, LeGoues et al. [24] studied the influence of crystallography upon critical nucleus shapes and kinetics of homogeneous nucleation by combining the discrete lattice mean-field model with the microscopic theory of strain energy. They considered both the influence of anisotropic interfacial energy and anisotropic strain energy on nucleation. However, they also assumed that the shapes of the critical nuclei were either spherical or plates.

In a recent letter, we reported a computational approach for predicting the morphology of a critical nucleus as an extreme state in two dimensions by considering the presence of both interfacial energy anisotropy and elastic interactions [39]. Some rigorous mathematical and numerical analysis of the underlying framework are discussed in Ref. [40]. The main purpose of this paper is to extend the model and the numerical implementation to three dimensions and discuss the influence of elastic energy on the morphology of critical nucleus and shape bifurcations as strain energy contribution increases. Though a particular example of cubic to cubic transformation within the homogeneous modulus approximation is considered, our approach can be generalized to other phase transformations. The key elements of such an approach involve the diffuse-interface description of the nucleation problem [1] and the minimax algorithm in the calculus of variation [30]. A detailed description on the theoretical formulation and numerical solutions is provided here. The effect of elastic energy contribution on the size and shape of a critical nucleus is studied. It is shown that strong elastic energy interactions may lead to critical nuclei with a wide variety of shapes, including plates, needles and cuboids with non-convex interfaces. It should be emphasized that the problem under consideration is spatially inhomogeneous and it is different from the saddle point search when a solid is homogeneously transformed to a near phase throughout the system, described by a homogeneous free energy as a function of a homogeneous order parameter.

The rest of the paper is organized as follows. The diffuse interface formulation of nucleation is presented in Section 2. The numerical algorithm for finding the critical nucleus and its computer implementation are described in Section 3. The spectral accuracy of the numerically computed solutions is validated in Section 4, along with a number of two-

dimensional and three-dimensional numerical simulations of the effect of elastic energy on nucleus morphology. The most probable nucleus morphology is identified for a given relative elastic energy and chemical driving force contributions. To offer additional understanding on the competition of interfacial and elastic energies, we also examine the various energy contributions analytically in a sharp interface limit. Some final conclusions are given in Section 5.

2. Diffuse interface model

Following Ref. [39], we consider the case of a structural transition with no compositional changes. It is further assumed that the structural difference between the parent phase and the nucleating phase can be sufficiently described by a single order parameter η . Extensions to more general cases, e.g. nucleation of a new phase in a solid solution, can also be considered in a similar fashion, and will be pursued in subsequent works.

For a given temperature, a double-well potential is chosen to describe the free energy dependence on η : $f(\eta) = (\eta^2 - 1)^2/4 - \lambda h(\eta)$. The two local energy wells are at $\eta = \pm 1$ and $h(\eta) = (3\eta - \eta^3)/2$ respectively, so that 2λ gives the bulk driving force for the phase transformation from the $\eta = -1$ state to the $\eta = +1$ state (as illustrated in Fig. 1).

The total free energy of an inhomogeneous system described by a spatial distribution of η could be written as

$$E = \int_{\Omega} (f(\eta) + \frac{\alpha}{2} |\nabla \eta|^2) dx$$

where α is the gradient energy coefficient in Ω for the isotropic interfacial energy, and the domain $\Omega = (-1, 1)^d$ is used with $d = 2$ or 3 being the space dimension and a periodic boundary condition is used for the order parameter η .

In the case that the interfacial energy is anisotropic, as is usually the case for nucleation in solids, either the gradient energy coefficient can be expressed as a second or higher order derivative or, rather artificially but common in the phase-field models, it is made directionally dependent. To incorporate the effect of long-range elastic interactions on the morphology of a critical nucleus and thus the nucleation barrier, the computation of the elastic energy E_{el} for an arbitrary microstructure is needed. Assuming that

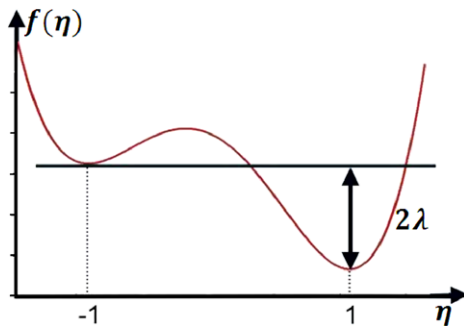


Fig. 1. A double well potential with wells at $\eta = \pm 1$ and the driving force being 2λ .

the elastic modulus is anisotropic but homogeneous, the microscopic elasticity theory of Khachaturyan [20] is often used in phase field simulations. For example, the elasticity effect is incorporated by expressing the elastic strain energy as a function of field variables (see the discussions in e.g. Refs. [4,37]). So the total energy is given by

$$E_{\text{total}} = \int_{\Omega} (f(\eta) + \frac{1}{2} \alpha |\nabla \eta|^2) dx + E_{el} \quad (1)$$

The elastic energy E_{el} is defined as

$$E_{el} = \frac{1}{2} \int_{\Omega} c_{ijkl} e_{ij} e_{kl} dx \quad (2)$$

where e_{ij} is the total strain and c_{ijkl} is the elastic stiffness tensor for $i, j, k, l = 1, 2, 3$. The summation convention for the repeated indices is employed in the above equation (2). For a cubic material with its three independent elastic constants c_{11} , c_{12} and c_{44} in the Voigt's notation, the elastic energy takes on the form [20]:

$$E_{el} = \int_{\Omega} \left\{ \frac{1}{2} c_{11} (e_{11}^2 + e_{22}^2 + e_{33}^2) + c_{12} (e_{11}e_{22} + e_{11}e_{33} + e_{22}e_{33}) + 2c_{44} (e_{12}^2 + e_{13}^2 + e_{23}^2) \right\} dx$$

Here, the elastic strain e_{ij} is the difference between the total strain ε_{ij} and stress-free strain ε_{ij}^0 since stress-free strain does not contribute to the total elastic energy, i.e.

$$e_{ij} = \varepsilon_{ij} - \varepsilon_{ij}^0$$

where the stress-free strain is

$$\varepsilon_{ij}^0 = \varepsilon_{ij}^*(\eta - \eta_0)$$

Here, ε_{ij}^* is a constant tensor and η_0 is the average order parameter of the system. The total strain ε_{ij} may be represented as the sum of homogeneous and heterogeneous strains:

$$\varepsilon_{ij} = \bar{\varepsilon}_{ij} + \delta \varepsilon_{ij}$$

The homogeneous strain is defined in such a way so that

$$\int_{\Omega} \delta \varepsilon_{ij} dx = 0$$

The heterogeneous strain is related to the local displacement field $\{u_k\}$ by the usual elasticity relation,

$$\delta \varepsilon_{ij} = \frac{1}{2} \left(\frac{\partial u_i}{\partial x_j} + \frac{\partial u_j}{\partial x_i} \right)$$

It also satisfies the mechanical equilibrium condition given by the equation

$$\frac{\partial \sigma_{ij}}{\partial x_j} = 0$$

with the stress components $\sigma_{ij} = c_{ijkl} e_{kl}$

The elasticity equation with periodic boundary conditions can be solved in the Fourier space which leads to a more explicit form of E_{el} . If there is a simply connected coherent inclusion in an anisotropic solid with cubic sym-

metry and the phase transformation involves only one type of crystal lattice, the elasticity energy contribution can be further simplified (see the details in Ref. [20,21]):

$$E_{\text{el}} = \frac{1}{2(2\pi)^d} \int_{\hat{\Omega}} d\mathbf{k} B(\mathbf{n}) |\hat{\eta}(\mathbf{k}) - \hat{\eta}_0(\mathbf{k})|^2 \quad (3)$$

The integration in (3) is over the reciprocal space $\hat{\Omega}$ of the reciprocal lattice vector \mathbf{k} , $\mathbf{n} = \mathbf{k}/|\mathbf{k}| = (n_1, n_2, n_3)$ is the normalized unit vector, and in three dimensions the term $B(\mathbf{n})$ is given by

$$B(\mathbf{n}) = 3(c_{11} + 2c_{12})\epsilon_0^2 - \frac{(c_{11} + 2c_{12})^2 \epsilon_0^2 (1 + 2\zeta s(\mathbf{n}) + 3\zeta^2 n_1^2 n_2^2 n_3^2)}{c_{11} + \zeta(c_{11} + c_{12})s(\mathbf{n}) + \zeta^2(c_{11} + 2c_{12} + c_{44})n_1^2 n_2^2 n_3^2} \quad (4)$$

where ϵ_0 is the lattice mismatch between the nucleating new cubic phase and the parent cubic phase, $\zeta = (c_{11} - c_{12} - 2c_{44})/c_{44}$ is the elastic anisotropic factor, and $s(\mathbf{n}) = n_1^2 n_2^2 + n_1^2 n_3^2 + n_2^2 n_3^2$.

Incorporating the long-range elastic interactions and a simple form of the surface energy anisotropy, the total free energy increase arising from the order parameter fluctuation in an initially homogeneous state with η_0 is given by

$$\Delta E_{\text{total}} = \int_{\Omega} \left(\delta f(\eta) + \frac{\alpha_x}{2} \eta_x^2 + \frac{\alpha_y}{2} \eta_y^2 \right) d\mathbf{x} + \frac{\beta}{2(2\pi)^d} \int_{\hat{\Omega}} d\mathbf{k} B(\mathbf{n}) |\hat{\eta}(\mathbf{k}) - \hat{\eta}_0(\mathbf{k})|^2 \quad (5)$$

where $\delta f(\eta) = f(\eta) - f(\eta_0)$. Instead of changing the magnitudes of lattice mismatch and elastic constants, a factor β is introduced which effectively characterizes the relative elastic energy contribution to the free energy driving force in determining the critical nucleus morphology.

3. Numerical algorithm

As nucleation can be achieved by overcoming the minimum energy barrier, a critical nucleus may be defined as the spatial order parameter fluctuation which allows the minimum free energy increase among all fluctuations which lead to nucleation. Such a scenario is consistent with the large derivation theory, which states that the most probable path (that minimizes the action [23]) passes through the saddle point in the large time limit. In the study here, our primary interest is to examine the effect of elastic energy contributions on the critical nucleus profiles, which can be found by computing the saddle point of the energy functional, of the order parameter η , that has the highest energy along the minimum action path.

By the usual calculus of variation, a saddle point is necessarily a solution of the Euler–Lagrange equation corresponding to the energy ΔE_{total} :

$$\alpha_x \frac{\partial^2 \eta}{\partial x^2} + \alpha_y \frac{\partial^2 \eta}{\partial y^2} = \frac{\partial}{\partial \eta} \delta f(\eta) + \frac{\beta}{(2\pi)^d} \int_{\hat{\Omega}} B(\mathbf{n}) (\hat{\eta}(\mathbf{k}) - \hat{\eta}_0(\mathbf{k})) e^{i\mathbf{k}\mathbf{x}} d\mathbf{k} \quad (6)$$

subject to the periodic boundary condition. Eq. (6) can be viewed as a nonlocal perturbation, due to the elastic contribution, to some well studied semi-linear elliptic equation [30]. We recall that there have been various approaches proposed for solving variational problems numerically which include, in particular, methods for the computation of saddle points and minimum energy paths [9,11,16,17,19,26]. While a couple of different approaches have been successfully implemented for the problem under consideration, the results reported here are based on the use of the minimax technique that has been studied extensively in calculus of variation and optimization [28,30]. Similar computational results have also been obtained via other approaches, further validating the computational findings presented in the later examples.

In less technical terms, the main idea of the minimax algorithm is to first define a solution submanifold \mathcal{M} such that a local minimum point of ΔE_{total} on \mathcal{M} yields a saddle point of the energy. Thus, the saddle point computation is effectively transformed into a minimization of ΔE_{total} on the submanifold, and a saddle point becomes stable on the submanifold \mathcal{M} . To ensure stability and monotonicity in the numerical procedure, a steepest descent search is applied to approximate a local minimizer of ΔE_{total} on the submanifold \mathcal{M} . Meanwhile, a *return rule* is used to prevent the descent search from leaving the submanifold so as to guarantee the convergence of the algorithm. While different versions of the minimax algorithm can be considered, we follow the approach studied by Li and Zhou [26], which is outlined below:

1. For $k = 0$, take a direction v_0 at a local minimum η_0 , define

$$\mathcal{M}_0 = \{\eta_0 + \text{span}\{v_0\}\}$$

and search for a local maximum of ΔE_{total} in \mathcal{M}_0 , i.e. solve

$$w^k = p(v_0) := \arg \max_{u \in \mathcal{M}_0} \Delta E_{\text{total}}(u).$$

2. For $k \geq 0$, compute the variational gradient g^k of ΔE_{total} at w^k . If $\|g^k\|$ is less than some tolerance, stop and output w^k as a critical nucleus, else goto Step 3.
3. For $\mathcal{M}_b^{k+1} = \{v_k + \text{span}\{v_b^k\}\}$ with b in $(0, \hat{b}_k)$ and v_b^k being the unit vector in the direction of $v^k - b g^k$, solve

$$p(v_b^k) := \arg \max_{u \in \mathcal{M}_b^{k+1}} \Delta E_{\text{total}}(u).$$

Then, solve

$$b^* := \arg \min_{0 < b < \hat{b}_k} \Delta E_{\text{total}}(p(v_b^k)),$$

set $v^{k+1} = v_{b^*}^k$, $w^{k+1} = p(v^{k+1})$, update k by $k + 1$ and goto step 2.

Earlier applications of the above algorithm often focus on well-known semi-linear elliptic equations in the calculus of variation. We refer to Ref. [26] for additional discussions

and the convergence properties. We hereby give some comments on the implementation of the above algorithm. First, with the periodic boundary condition, the non-locality due to the elastic contributions can be efficiently treated in the Fourier space, thus a Fourier spectral method becomes appropriate when the minimax algorithms are implemented in the numerical computation [2,40]. Secondly, to enhance the computational efficiency, we find that it works well to choose a tanh profile as the initial search direction in the first step. The argument of such a tanh function is a scaled distance to some prescribed level set. Thirdly, in Step 2, the number \hat{b}_k is used to control the step-size of the steepest descent search, which is important for the stability of the algorithm.

Furthermore, the Fourier spectral method has been proven to be highly accurate and efficient. More theoretical analysis and numerical tests of the discretization can be found in [40]. Moreover, in the second step, in order to accelerate the convergence, we adopt the so-called H^1 inner product for the definition of the variational gradient g^k . Such an inner product of any two functions is given by the integral of the sum of their product and the product of their gradients. This effectively defines the variational gradient of the energy functional in the so-called H^{-1} sense which is a dual space of H^1 and is often used in energy minimizations [7,8,36]. In our case, the computation of the variational gradient is particularly convenient as it can be computed again via FFT in the Fourier spectral discretization.

In addition, we also note that, depending on the choice of the initial profiles, several different saddle points may be found. As is often the case for solving nonlinear equations, we take a parameter continuation approach (with respect to the parameter β , in particular) to compute the various

solution branches for the saddle points. The critical nuclei may be identified, for a particular parameter value, by comparing the energy of the saddle points on the different branches. While it may not be possible to exhaustively search for all possible saddle points, efforts are made to use many different initial profiles to ensure that those with lower energy values are successfully found in the numerical computation.

4. Computer simulations

A number of computer simulations are carried out in order to make predictions on the critical nucleus morphologies based on the developed model and the numerical algorithm. Here, results of both two-dimensional and three-dimensional simulations are reported for the particular example of cubic to cubic transformation within the homogeneous modulus approximation.

For the case of the interfacial energy anisotropy, we find that the predicted critical profile displays the ellipsoidal direction-dependence as one would expect from the interfacial energy anisotropy (see the details in [39]). To examine the effect of the elastic contributions, we plot the predicted critical profiles in the presence of the long-range elastic interactions in Fig. 2. The parameter values used in the simulations are given by $\eta_0 = -1$, $\alpha_x = \alpha_y = 2.44 \times 10^{-4}$, $\lambda = 0.0469$ and $c_{11} = 250$, $c_{12} = 150$, $c_{44} = 100$, $\epsilon_0 = 0.01$. The critical order parameter profiles are plotted for $\beta = 0.16, 0.63$ and 0.78 respectively. As shown in Fig. 2, long-range elastic interactions can dramatically change the critical nucleus morphology. A strong elastic interaction may lead to critical nuclei with cuboidal, plate-like, or even possibly of non-convex shapes, which are signature properties due to the anisotropic elastic energy

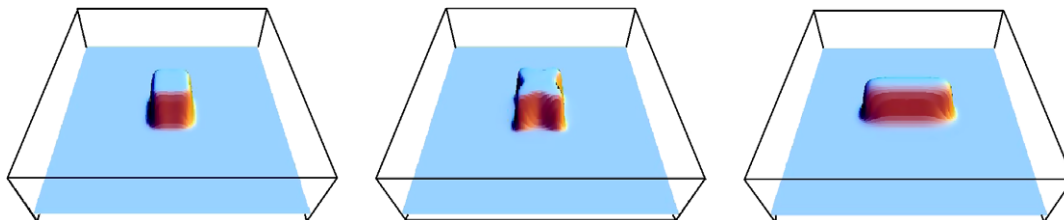


Fig. 2. Plots of the order parameter profiles corresponding to the two-dimensional critical nuclei shapes in a cubically anisotropic system with $\beta = 0.16, 0.63$, and 0.78 , respectively.

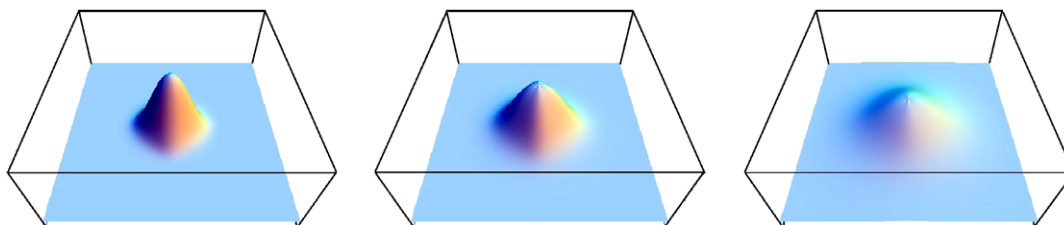


Fig. 3. Plots of the order parameter profiles corresponding to two-dimensional critical nuclei shapes with the diffuse interface width taken to be $0.06, 0.1$ and 0.15 , respectively.

contribution. Similar findings and more discussions on the two-dimensional computation are given in Ref. [39]. Furthermore, some evidence on the convergence and spectral accuracy of the numerical solution could be found in Ref. [40].

To see the effect of the diffuse interfacial width, in Fig. 3 we take $c_{11} = 250$ and $c_{12} = c_{44} = 50$, and plot, respectively the critical nucleus profiles computed with different values of interfacial width corresponding to 0.06 and 0.1 – 0.15. It can be seen that the interfaces diffuse more with larger interfacial width. Due to the elastic interactions, the shapes of the critical nuclei are also no longer completely circular.

Finally, we present some simulations of the three-dimensional critical nuclei and examine the effect of relative elastic energy contribution. The simulation results were obtained on a 64^3 three-dimensional computational grid. The Figs. 4 and 5 contain computed isosurface plots of saddle point profiles corresponding to different elastic energy contributions. In Fig. 4, we take $c_{11} = 250$, $c_{12} = 150$, $c_{44} = 100$, $\epsilon_0 = 0.01$, $\eta_0 = -1$, $\alpha_x = \alpha_y = 9.7656 \times 10^{-4}$ and $\lambda = 0.1563$. In Fig. 5, the same parameter values are used except for λ . In this case, $\lambda = 0.3125$ is used to avoid making the size of the critical nucleus too large to fit in the domain Ω .

Similar to the previous findings based on the two-dimensional computational results, the critical nuclei could be cuboidal, plate-like, and non-convex shapes. In addition, we find that the long-range elastic interaction may also lead

to critical nuclei with needle shapes. To describe the three-dimensional most probable nucleus morphology for a given relative elastic energy and given chemical driving force contributions, we plot in Fig. 6 (right) the formation energy of the saddle point profiles for different values of β with the same parameters as in Fig. 5. The circles, triangles and diamonds are data points based on the computed critical order parameter profiles, while the solid and dash curves are the least square fits of these data points by cubic polynomials. For small β , the critical nuclei with lower energy possess the symmetry of a cubic crystal, i.e. they are either nearly spherical or take on shapes like a cube with rounded corners. As β increases to above 0.94, the nucleus becomes non-convex. For even larger β (above 1.4), while one saddle point curve maintains the cubic symmetry, there is a second curve of saddle points with lower energy values corresponding to nuclei having lower symmetry groups. Continuing the latter curve for smaller β below the intersection point shows that it leads to saddle points of higher energy than that for the non-convex, cube-like and nearly circular nuclei. For some intermediate values of β , we again confirm, through our three-dimensional simulation, the surprising result of critical nuclei with non-convex surfaces being the most probable morphology as previously observed in two dimensions [39]. It should be noted that this conclusion is reached by ignoring the possible presence of defects such as dislocations and interfaces, i.e. heterogeneous nucleation.

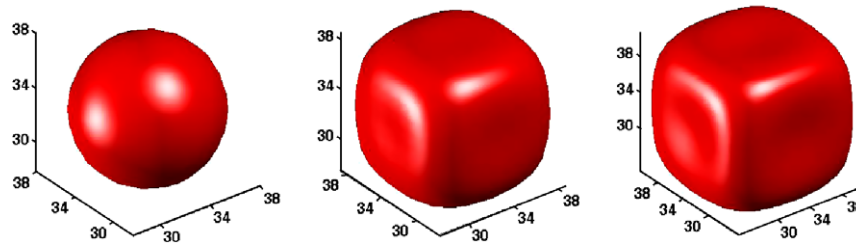


Fig. 4. Isosurface plots of the order parameter profiles corresponding to the three-dimensional saddle point for $\beta = 0, 0.63$, and 1.25 , respectively.

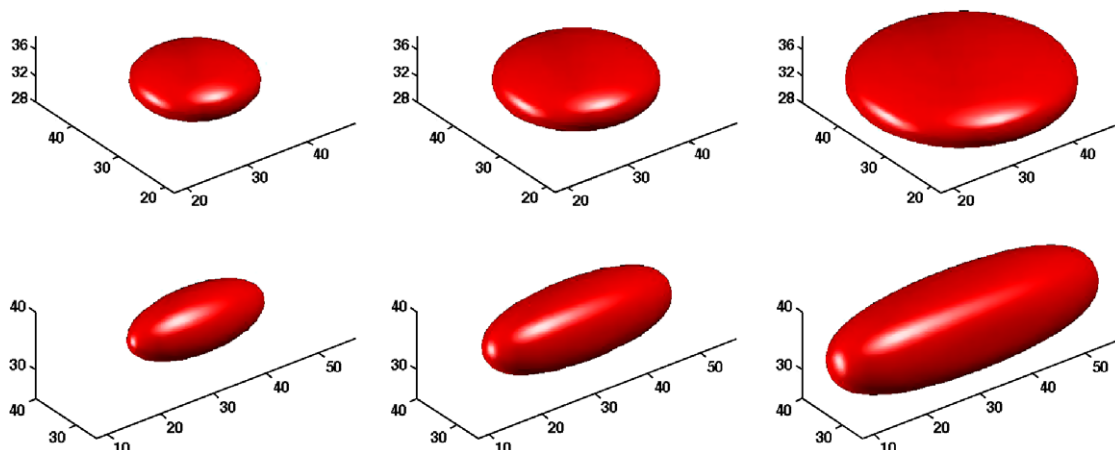


Fig. 5. Isosurface plots of the order parameter profiles corresponding to three-dimensional saddle points of the plate (top row) and needle (bottom row) shapes for $\beta = 0.31, 0.94$, and 1.56 , respectively.

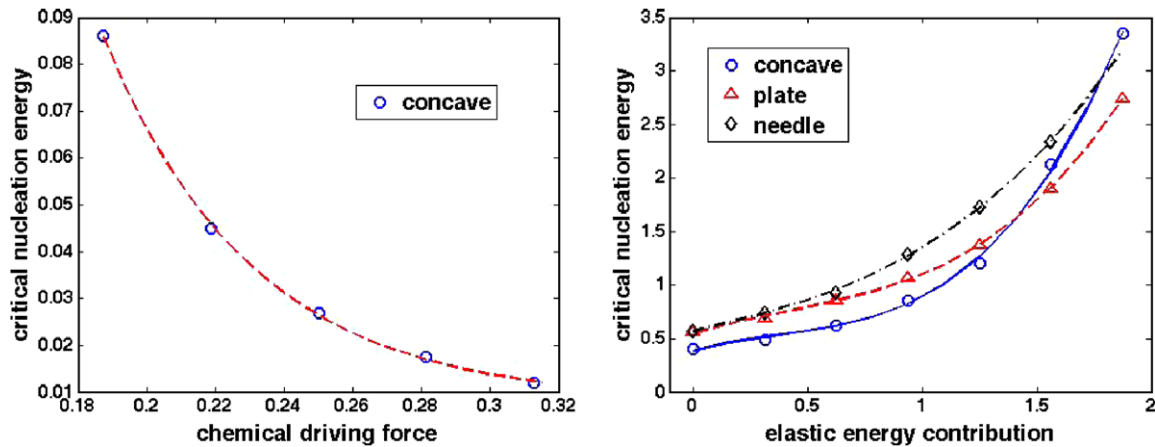


Fig. 6. Plots of the three-dimensional critical nucleation energy with respect to the changing driving force at $\beta = 1.25$. (left) and the changing elastic energy contribution (right) at $\lambda = 0.3125$. The circles, triangles and diamonds represent data points based on the computed critical order parameter profiles, while the solid and dashed curves are the least-squares fits.

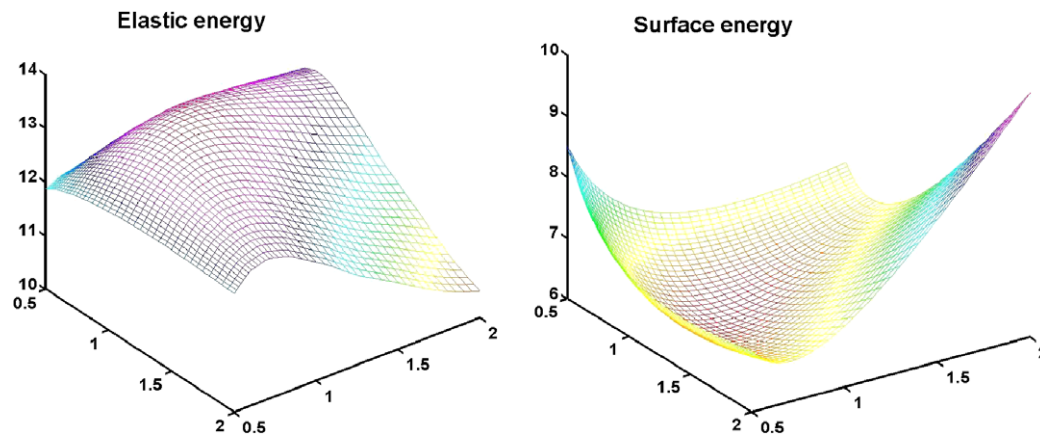


Fig. 7. Surface plots of the elastic energy (left) and the surface energy (right) as a function of the length and width associated with for cuboidal shapes with the unit volume.

Fig. 6 (left) plots the critical free energy of formation as a function of bulk chemical driving forces λ with a fixed $\beta = 1.25$. The blue circles represent the data points for the computed non-convex-shape critical nuclei, and the red dash curve is a least-squares fit by an exponential function. As expected, with the increase in the driving force, the size of critical nuclei (of cubic symmetry) is reduced and the critical free energy decreases. This dependence is similar to that predicted from the classical nucleation theory for spherical particles.

The profiles computed are verified to indeed besaddle points, as discussed in Ref. [39]. Thus, we observe that, with a stronger elastic energy contribution, the formation energy for a critical nucleus with a lower symmetry is lower than that with cubic symmetry but with non-convex interfaces. Meanwhile, we notice that, in the example computed here, the critical nucleation energy of the needle-shape nucleus is always higher than that of plate-shape nuclei corresponding to the same parameters. To gain a better understanding on the competition of the elastic and interfacial

energies, we consider the three-dimensional analog of the discussions for the two-dimensional case given in Ref. [39] and compare the energies in Fig. 7 for cuboid nuclei of dimensions a, b and $1/(ab)$ with changing aspect ratios. To make the calculation analytically tractable, we carry out the calculation of the various energies, albeit in the sharp interface limit of the diffuse interface model. That is, we let η be a Heaviside function with ± 1 inside and outside the cuboid with its Fourier coefficients given by

$$\hat{\eta}(\mathbf{k}) = \frac{\sin(\pi k_x a) \sin(\pi k_y b) \sin(\pi k_z / (ab))}{\pi^3 k_x k_y k_z}$$

Substituting it into Eq. (5), we can get an estimation of the elastic energy in Fig. 7 (right). The sharp surface energy, meanwhile, is proportional to $2(ab + 1/a + 1/b)$ in Fig. 7 (left). These calculations indicate how the different energies are affected by the aspect ratio in the sharp interface limit and we may expect similar effects remain in the diffuse interface formulation. It is clear that the surface energy is the smallest for $a = b = 1$ (thus preferring the cubic sym-

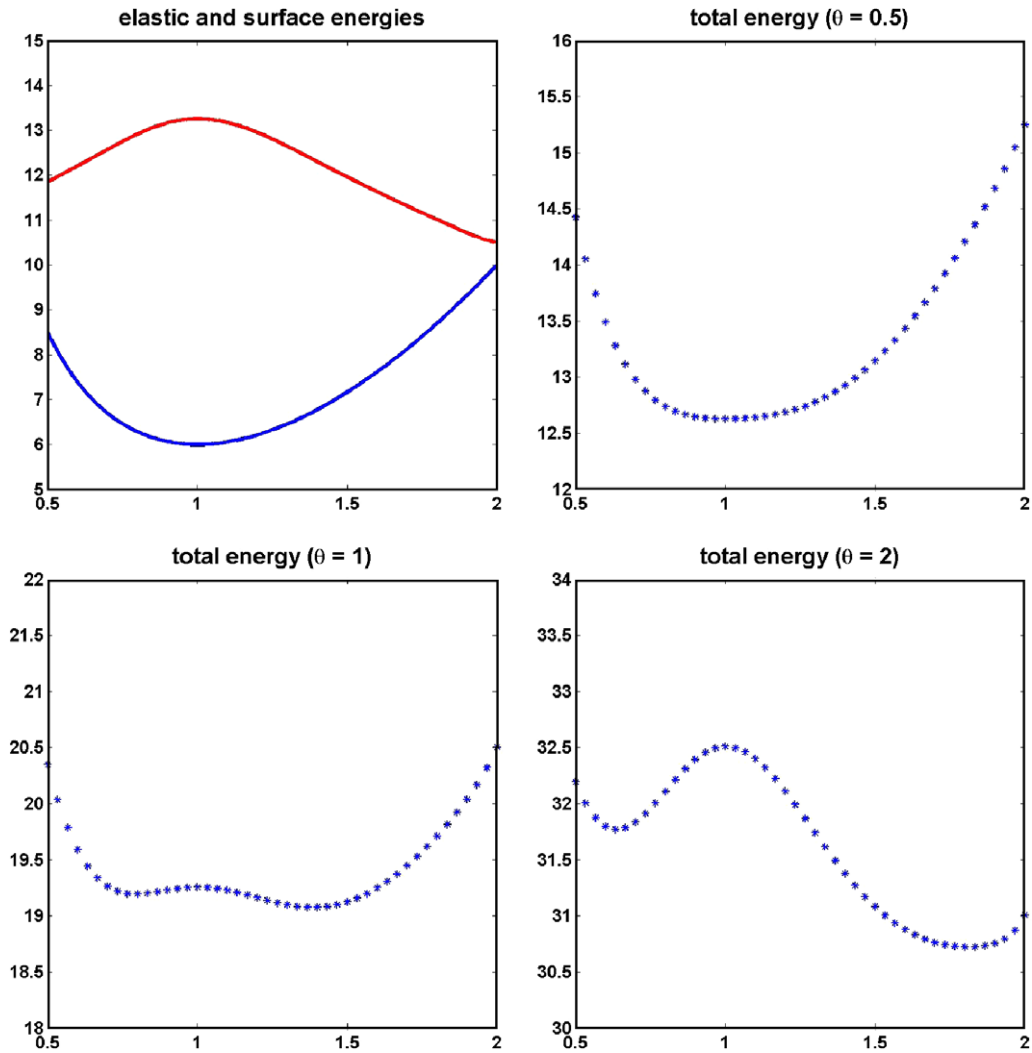


Fig. 8. Plots of the surface and elastic energies (top left) and the total energy with the coefficient $\theta = 0.5, 1$ and 2 respectively as a function of a for cuboidal shapes of size $a \times a \times 1/a$.

metry), while the elastic energy is lower with high aspect ratios corresponding to either plate or needle shapes.

The three-dimensional geometry leads to two possible configurations with lower symmetry. To see which lower symmetry is more probable, we further examine the surface energy and the elastic energy for some artificially constructed plate-like and needle-like shapes. We take the cuboid nuclei of dimension a, a and $1/a^2$ and consider local minimizers over this special class of possible shapes, with $a > 1$ being close to a plate-like shape and $a < 1$ resembling to a needle-like shape. We calculate the surface and elastic energies and choose a linear combination of two energies via a factor θ as the total energy $E_{\text{total}} = E_{\text{surface}} + \theta \cdot E_{\text{el}}$. In Fig. 8, the surface, elastic and total energies are plotted with different values of θ . We notice that, as θ is small, the total energy has a minimizer around $a = 1$, so the cubic symmetry is preferred. As θ increases to above 1, the total energy has two local minimizers at $a < 1$ and $a > 1$. The minimum energy at $a > 1$ is lower than that at $a < 1$, which means the plate-shaped nuclei are more probable than the

needle-shaped nuclei. Although this calculation is for the sharp interface approximation of the a priori given shapes, it does offer a hint on the relation between needle shapes and plate shapes due to the competition between the interfacial and elastic energies. The diffuse-interface model captures this competition and effectively distinguishes the parameter ranges where one energy dominates the other, so that critical nuclei with the particular lower symmetry are identified as the most probable profiles for larger elastic energy contributions.

5. Conclusion

In this paper, a recently proposed diffuse interface approach for the study of critical nuclei morphologies in elastically anisotropic solids is discussed. The model and numerical implementation are extended to the three-dimensional cases and the influence of elastic energy on the morphology of critical nucleus and shape bifurcations is demonstrated as the strain energy contribution increases.

Expanded discussions are provided on the background, models and algorithms, numerical convergence tests and numerical examples, along with sharp interface comparisons of the various energy contributions. Through the diffuse interface calculations, some fascinating observations are illustrated in three dimensions on the presence of nuclei with non-convex shapes, and the formation of critical nuclei whose symmetry is lower than both the new phase and the original parent matrix. Additional insights into these numerically observed phenomena are offered via some simple analytical calculations in the sharp interface limit. Although there have been extensive theoretical studies of particle morphologies during growth or coarsening by minimizing the total interfacial and elastic strain energy [3,6,10,13,25,34,37], our method provides a new approach for the prediction of the morphologies of saddle-point critical nuclei without any a priori assumptions on the shapes. This approach can also be applied to nucleation of new phase particles in solid solutions, non-cubic systems, as well as to systems with defects such as dislocations and interfaces, i.e. heterogeneous nucleation.

Acknowledgements

This work is supported in part by NSF-DMR ITR 0205232, NSF-DMS 0712744 and by NSF-IIP 541674 Center for Computational Materials Design (CCMD). The authors would like to acknowledge the valuable suggestions made by the referee.

References

- [1] Cahn J, Hilliard J. *J Chem Phys* 1959;31:688–99.
- [2] Chen LQ, Shen J. *Comput Phys Commun* 1998;108:147–58.
- [3] Chen LQ. *Annu Rev Mater Sci* 2002;32:113–40.
- [4] Chen LQ, Wang YZ, Khachaturyan AG. *Philos Mag Lett* 1991;64:241–51.
- [5] Chu Y, Moran B, Reid A, Olson G. *Metal Mater Trans A* 2000;31:1321–31.
- [6] Conti S, Schweizer B. *Arch Rat Mech Anal* 2006;179:413–52.
- [7] Du Q, Gunzburger M, Peterson J. *SIAM Rev* 1992;34:54–81.
- [8] Du Q, Liu C, Wang X. *J Comput Phys* 2004;198:450–68.
- [9] Ren W, E W, Vanden-Eijnden E. *Phys Rev B* 2002;66:052301.
- [10] Eshelby J. *Proc Roy Soc London A* 1959;252:561–9.
- [11] Fischer S, Karplus M. *Chem Phys Lett* 1992;194:252–61.
- [12] Gagne C, Gould H, Klein W, Lookman T, Saxena A. *Phys Rev Lett* 2005;95:095701.
- [13] Garcke H, Rumpf M, Weikard U. *Interfaces Free Boundaries* 2001;3:101–18.
- [14] Granasy L, Pusztai T, Borzsonyi T, et al. *J Mater Res* 2006;21:309–19.
- [15] Granasy L, Pusztai T, Saylor D, et al. *Phys Rev Lett* 2007;98:035703.
- [16] Henkelman G, Jonsson H. *J Chem Phys* 1999;111:7010–22.
- [17] Henkelman G, Uberuaga B, Jonsson H. *J Chem Phys* 2000;113:9901–4.
- [18] Hu SY, Chen LQ. *Acta Mater* 2001;49:463–72.
- [19] Ionova I, Carter E. *J Chem Phys* 1993;98:6377–86.
- [20] Khachaturyan A. *Theory of Structural Transformations in Solids*. New York: Wiley; 1983.
- [21] Khachaturyan AG, Shatalov GA. *Sov Phys Solid State, USSR* 1969;11:118–23.
- [22] Khachaturyan AG, Suris RA. *Sov Phys Crystallogr, USSR* 1968;13:83–9.
- [23] Kohn R, Reznikoff M, Tonegawa Y. *Calc Var PDEs* 2006;25:503–34.
- [24] Legoues FK, Aaronson HI, Lee YW. *Acta Metall* 1984;32:1845–53.
- [25] Li X, Thornton K, Nie Q, Voorhees P, Lowengrub J. *Acta Mater* 2004;52:5829–43.
- [26] Li Y, Zhou J. *SIAM J Sci Comp* 2001;23:840–65.
- [27] Luo W, Shen C, Wang Y. *Acta Mater* 2007;55:2579–86.
- [28] Moré J, Munson T. *Math Prog* 2004;100:151–82.
- [29] Poduri R, Chen LQ. *Acta Mater* 1996;44:4253–9.
- [30] Rabinowitz P. *Minimax Methods in Critical Point Theory With Applications to Differential Equations*. Providence: AMS; 1986.
- [31] Roitburd AL. *Mater Sci Eng, A* 1990;127:229–38.
- [32] Roitburd AL, Khachaturyan AG, Plaksina TS. *Sov Phys Solid State, USSR* 1969;10:1684–6.
- [33] Roy A, Rickman J, Gunton J, Elder K. *Phys Rev E* 1998;57:2610–7.
- [34] Sagui C, Somoza AM, Desai R. *Phys Rev E* 1994;50:4865–79.
- [35] Shen C, Simmons JP, Wang Y. *Acta Mater* 2007;55:1457–66.
- [36] Sial S, Neuberger J, Lookman T, Saxena A. *J Comput Phys* 2003;189:88–97.
- [37] Wang Y, Chen LQ, Khachaturyan AG. *Acta Mater* 1993;41:279–96.
- [38] Wang Y, Khachaturyan A. *Acta Mater* 1997;45:759–73.
- [39] Zhang L, Chen LQ, Du Q. *Phys Rev Lett* 2007;98:265703.
- [40] Zhang L, Chen LQ, Du Q. *J Sci Comput*, in press.
- [41] Zhang W, Jin YM, Khachaturyan AG. *Acta Mater* 2007;55:565–74.